Annals of Biomedical Engineering, Vol. 35, No. 12, December 2007 (© 2007) pp. 2168–2179
DOI: 10.1007/s10439-007-9381-z

Blind Source Separation of Concurrent Disease-Related Patterns from EEG in Creutzfeldt–Jakob Disease for Assisting Early Diagnosis

CHIH-I HUNG,[1,2] PO-SHAN WANG,[3,4,6] BING-WEN SOONG,[3,4] SHIN TENG,[1,2] JEN-CHUEN HSIEH,[2,5] and YU-TE WU[1,2,5]

[1]Department of Biomedical Imaging and Radiological Sciences, National Yang-Ming University, No. 155, Section 2, Li-Nong Street, Bei-Tou, Taipei 112, Taiwan, ROC; [2]Integrated Brain Research Laboratory, Department of Medical Research and Education, Taipei Veterans General Hospital, Taipei, Taiwan, ROC; [3]The Neurological Institute, Taipei Veterans General Hospital, Taipei, Taiwan, ROC; [4]Department of Neurology, National Yang-Ming University School of Medicine, Taipei, Taiwan, ROC; [5]Institute of Brain Science, National Yang-Ming University, Taipei, Taiwan, ROC; and [6]The Neurological Institute, Taipei Municipal Gan-Dau Hospital, Taipei, Taiwan, ROC

(Received 14 December 2006; accepted 6 September 2007; published online 22 September 2007)

Abstract—Creutzfeldt–Jakob disease (CJD) is a rare, transmissible and fatal prion disorder of brain. Typical electroencephalography (EEG) patterns, such as the periodic sharp wave complexes (PSWCs), do not clearly emerge until the middle stage of CJD. To reduce transmission risks and avoid unnecessary treatments, the recognition of the hidden PSWCs forerunners from the contaminated EEG signals in the early stage is imperative. In this study, independent component analysis (ICA) was employed on the raw EEG signals recorded at the first admissions of five patients to segregate the co-occurrence of multiple disease-related features, which were difficult to be detected from the smeared EEG. Clear CJD-related waveforms, i.e., frontal intermittent rhythmical delta activity (FIRDA), fore PSWCs (triphasic waves) and periodic lateralized epileptiform discharges (PLEDs), have been successfully and simultaneously resolved from all patients. The ICA results elucidate the concurrent appearance of FIRDA and PLEDs or triphasic waves within the same EEG epoch, which has not been reported in the previous literature. Results show that ICA is an objective and effective means to extract the disease-related patterns for facilitating the early diagnosis of CJD.

Keywords—Frontal intermittent rhythmical delta activity (FIRDA), Periodic sharp wave complexes (PSWCs), Periodic lateralized epileptiform discharges (PLEDs).

INTRODUCTION

Creutzfeldt–Jakob disease (CJD) is a rare prion disorder of brain, with an approximated incidence of 0.5–1 case per million persons per year. The subtypes of human prion diseases can be familial, sporadic, or acquired, which are characterized by combination of clinical findings such as duration of disease, EEG changes, age at onset and predominant neurological signs. Sporadic CJD (sCJD) is the most common subtype of CJD that usually develops in the 5th to 7th decade of life, with a mean age of onset of 62 years old (median 65). Survival times ranging from 1 to 58 months have been reported.[24] The clinical presentations, such as memory loss, visual disturbances, involuntary movements, myoclonus, dementia, and coma can be observed subsequently from early to the terminal stage of the disease. Since CJD is a rapidly progressive, uniformly fatal and transmissible spongiform encephalopathy, detection of the CJD symptom in the early stage is crucial to avoid the fatal transmission.

Electroencephalography (EEG), cerebral magnetic resonance imaging (MRI), and cerebrospinal fluid analysis (CSF analysis) are currently the most common diagnostic means of CJD. To evaluate these techniques, Collins *et al*. investigated the influence of several clinical parameters, such as prion protein gene codon 129 polymorphism, molecular sub-type, age at disease onset, and illness duration, on the diagnostic sensitivity to EEG, cerebral MRI, and the CSF analysis. They reported that the CSF analysis had the highest sensitivity for early diagnosis since the 14-3-3 protein could be detected from the CSF after the disease had onset.[4] However, Geschwind *et al*. concluded that the sensitivity of CSF analysis in their study was only 53% and advised that it was risky to exclude the diagnosis of CJD in the case of negative CSF results.[7] Besides, the use of CSF 14-3-3 analysis, regardless of methods, is problematic since universally accepted standards are not available for performing such tests.

Address correspondence to Yu-Te Wu, Department of Biomedical Imaging and Radiological Sciences, National Yang-Ming University, No. 155, Section 2, Li-Nong Street, Bei-Tou, Taipei 112, Taiwan, ROC. Electronic mail: ytwu@ym.edu.tw

Magnetic resonance brain imaging is another developing tool for detecting CJD. The study conducted by the Schröter *et al.* revealed T2-weighted MRI alternations in 109 (67%) out of 162 sCJD patients,[20] whereas the sensitivity of abnormal T2-weighted or diffusion-weighted MRI reported by Collins *et al.* was 43%.[4] Accordingly, efforts to develop more effective techniques for the aid to early diagnosis are of potentially great importance.

EEG is one of the major techniques used to diagnose CJD and has been included in the World Heath Organization diagnostic classification criteria.[24] In general, EEG patterns of sCJD exhibit longitudinal changes along with the course of the disease, ranging from frontal intermittent rhythmical delta activity (FIRDA), i.e., slow waves with 1–3 Hz, in the early stage to periodic lateralized epileptiform discharges (PLEDs) or prototypical periodic sharp wave complexes (PSWCs) in the middle and late stages.[1,3,6,25] The temporal waveforms and the spatial dominances of FIRDA, PLEDs, and PSWCs are presented in the Figs. 1a and 1b, respectively. The morphology of PLEDs shows complexes, which consist of a bi- or multiphasic spike or sharp wave and may include a slow wave.[5] The PSWCs mainly comprise simple sharp waves, i.e., monophasic, biphasic, and triphasic waves, with a typical duration of 200–600 ms, although complexes with mixed spikes, polyspikes, and slower waves may appear from times to times.[5,24,25] The peak-to-peak intervals of PSWCs are usually between 0.5 and 2 s. The major difference between the PLEDs and PSWCs is their topographical dominances. The former is more hemispherically lateralized while the latter is more focal in the early stage and becomes diffusive after the middle stage. Since the PSWCs are not evident until the middle or late stage, detection of the PSWCs predecessors, such as FIRDA, PLEDs, and focal tirphasic waves, hidden in the smeared EEG signals is critical for the early diagnosis.

EEG recordings are overlapping potentials contributed from individual neurons inside the brain as well as from the artifacts produced outside the brain.[5] Figures 2b–4b illustrate parts of typical segments of raw EEG signals recorded from the first admissions of patient 1 (the early stage of CJD). The shaded areas show that the brain activities are severely contaminated by significantly large eye-movement potentials and environmental noises, which makes the visual inspection of FIRDA, PLEDs, and tirphasic waves in the early stage of CJD a difficult task.

To recover the CJD-related patterns from EEG data, we employed the independent component analysis (ICA)[11,23] in this study. ICA has been successfully applied to remove non-physiological artifacts from EEG data,[14,15] to segregate Rolandic beta rhythm from magnetoencephalographic (MEG) measurements of the right index finger lifting,[17] to extract the task-related features from the motor imagery EEG and the flash visual evoked EEG in the studies of the brain computer interface,[10,18] to analyze the interactions during temporal lobe seizures in stereotactic depth EEG,[22] to separate generalized spike-and-wave discharges into the primary and secondary bilateral synchrony,[13] and to segment spatiotemporal hemodynamics from perfusion magnetic resonance brain images.[16]

PATIENTS AND EEG RECORDINGS

Five patients (all male) with sCJD, aged 73, 74, 85, 52, and 80 years old were recruited in this study (for

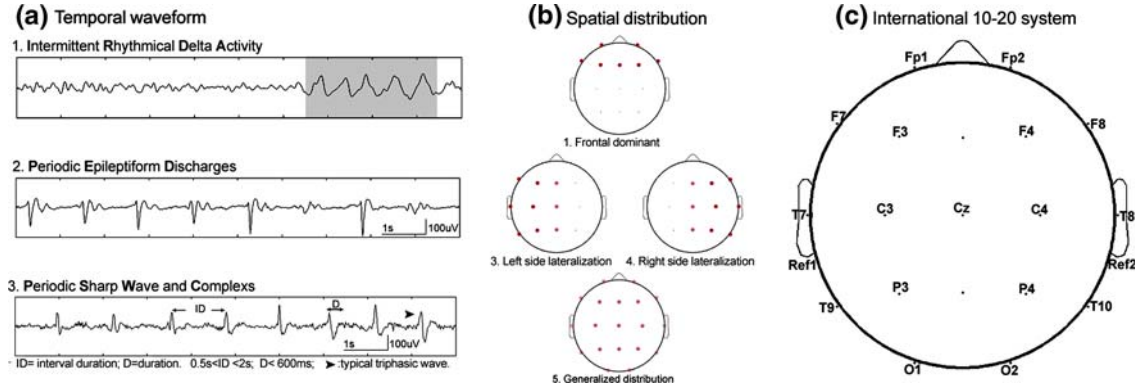

FIGURE 1. (a) Temporal waveforms of FIRDA, PLEDs, and PSWCs. The PLEDs mainly consist of a bi- or multiphasic spike or sharp wave. The PSWCs mainly comprise simple sharp waves, i.e., monophasic, biphasic, and triphasic waves, with a typical duration of 200–600 ms and the peak-to-peak intervals are usually between 0.5 and 2 s. (b) Spatial dominances of FIRDA, PLEDs, and PSWCs. The FIRDA is usually observed in the frontal areas, the PLEDs are hemispherically lateralized, and the PSWCs are usually more focal in early stage and become diffusive after middle stage. (c) The whole scalp of each subject was covered with 17 EEG electrodes placed onto anatomical locations according to the international 10–20 system, where Fp, F, C, P, O, and T represent the abbreviations of frontal polar, frontal, central, parietal, occipital, and temporal, respectively.

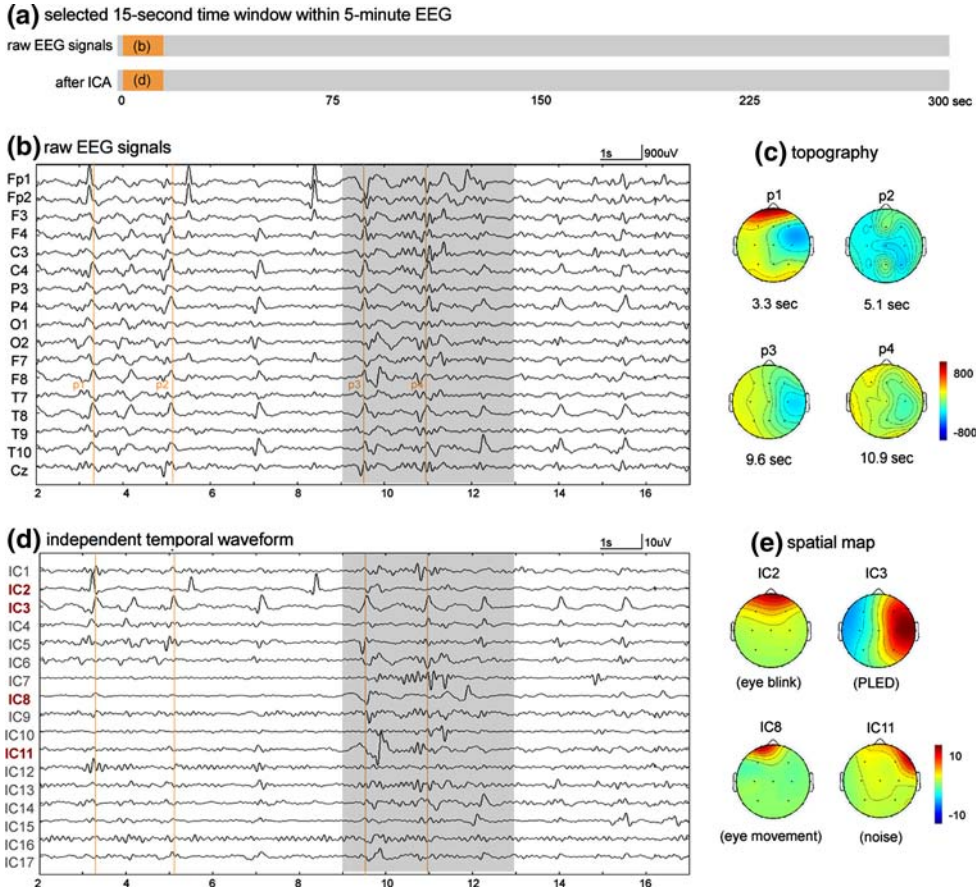

FIGURE 2. The first selected EEG segment and ICA results from patient 1. Once W and S were resolved by ICA (Eq. 5), rows of S representing the temporal waveforms of independent sources were displayed in (d), and each column of W^{-1} denoting the relative (spatial) weightings of each sources was depicted as a topography map in (e). (a) A 15-s time window (2–17 s) within 5-min data used to display results in (b) and (d). (b) The illustration of a 15-s segment where signals in the shaded areas were severely contaminated by large eye movements and environmental noises. (c) The topographical maps generated at four peak time points p1, p2, p3 and p4 (vertical lines in b) of four waves in IC3 at 3.3, 5.1, 9.6, and 10.9 s. (d) The 17 decomposed ICs show that diseased-related pattern was PLEDs (IC3) and the artifacts were eye blinks (IC2), eye movements (IC8), and noise (IC11). (e) The corresponding spatial maps of IC2, IC3, IC8, and IC11.

details, see Table 1). All of them met the criteria of probable CJD defined by WHO, were examined by board-certified neurologists, and underwent extensive diagnostic workups, including clinical, neurophysiological, neuroradiological examinations, and the CSF analysis. Disease onset was determined retrospectively based on history and clinical presentations as reported by the patients themselves and their relatives. The onset times of patient 1 to patient 5 were 6, 9, 4, 5, 3 weeks, respectively, before the first EEG recording. The EEGs were acquired using a 19-channel Nicolet EEG system (digitized at 250 Hz) with Ag/AgCl surface electrodes, which were placed based on the configuration of the international 10–20 system (Fig. 1c). We used the referential montage, rather than the bipolar or standard EEG, because the EEG signals can be expressed as $\mathbf{X} = \mathbf{AS\text{-}Ref}$ so that the mixing matrix can be obtained directly from FastICA (the **Ref** term was eliminated in the zero-mean pre-processing of FastICA). The use of bipolar montage would make the recovery of the mixing matrix much more difficult since the bipolar EEG signals are formulated as $\mathbf{X} = (\mathbf{A_1} - \mathbf{A_2})\mathbf{S}$ with the additional constrain $\mathbf{A_1}(i,j) = \mathbf{A_2}(i,j+1)$. Five-minute EEG recording was clipped for each subject, which was bandpass filtered between 0.5 and 10 Hz prior to the ICA process. In this study, the infinite impulse response (IIR) digital filter was designed based on the Butterworth magnitude response

$$|P_L(\mathbf{\Omega})| = \frac{1}{\sqrt{1+\mathbf{\Omega}^{2L}}}, \quad 1 \le L \tag{1}$$

where $\mathbf{\Omega}$ was the analog frequency and L was the order of the normalized low-pass analog filter.[21] Furthermore, the associated s-plane poles were given by

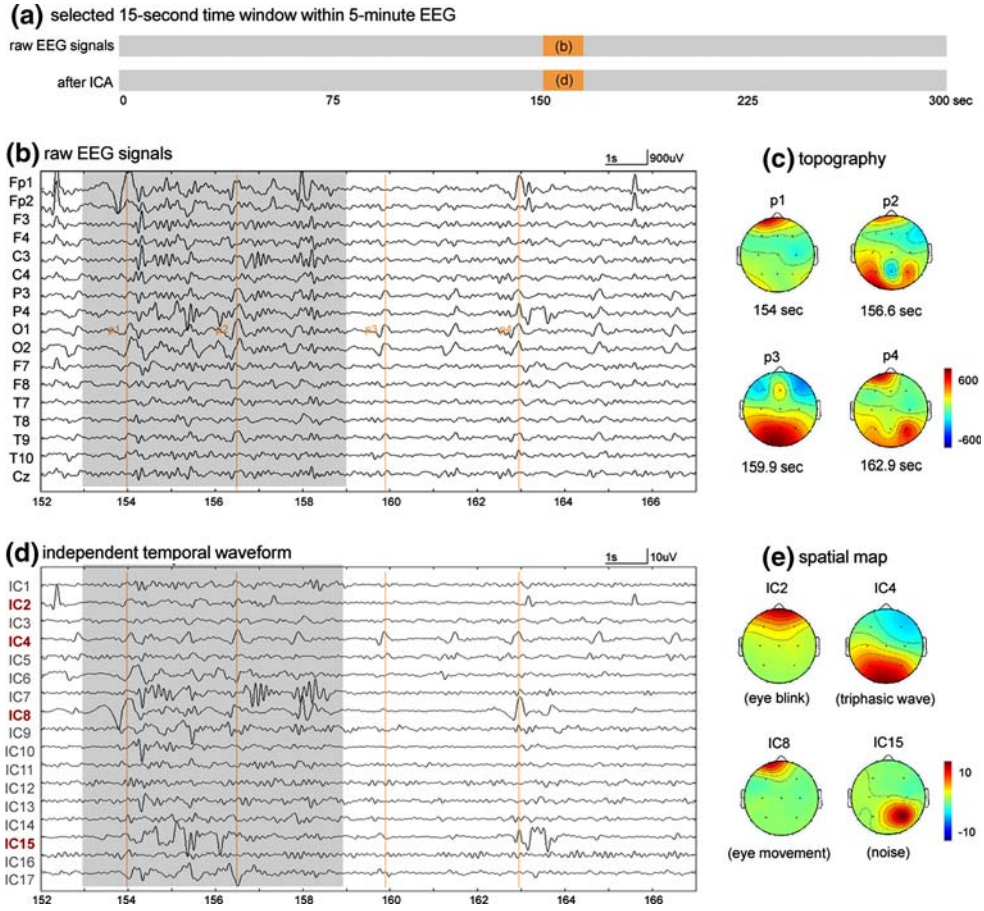

FIGURE 3. The second selected EEG segment and ICA results from patient 1. (a) The 15-s time window (152–167 s) used to display results in (b) and (d). (b) The illustration of a 15-s segment where signals in the shaded areas were severely contaminated by large eye movements and environmental noises. (c) The topographical maps generated at four peak time points p1, p2, p3 and p4 (vertical lines in b) of four waves in IC4 at 154, 156.6, 159.9, and 162.9 s. (d) The 17 decomposed ICs show that diseased-related pattern was focal triphasic waves (IC4) and the artifacts were eye blinks (IC2), eye movements (IC8) and noise (IC15). (e) The corresponding spatial maps of IC2, IC4, IC8, and IC15.

$$s_k = \exp\left(\frac{j(2k + L - 1)\pi}{2L}\right), \quad 1 \le k \le 2L. \qquad (2)$$

The bandpass filtering of the EEG was performed by the 6th-order high pass filter followed by the 16th-order low pass filter, which were implemented using MATLAB build-in functions.

Figure 2b displays a 15-s waveform of the 17-channel EEG (excluding two referential electrodes, Ref1 and Ref2) from one patient. We selected several time points at which the negative peaks or positive peaks (Figs. 2b–4b) in conjunction with the corresponding topographic maps (Figs. 2c–4c) which may possess some physiological meanings. However, due to the mixture of source signals, such as disease-related waveforms, environmental noises, and eye-movement artifacts, the disease-related compartments can be barely discerned either from the waveforms or from the topographic maps. It should be noted that the 15-s time windows showed in the Figs. 2–4 were selected merely to demonstrate such obscure mixture in the raw EEGs (Figs. 2b–4b). In our implementation, ICA was applied to the whole 5-min recording of each patient and the selection of the interval of interest prior to ICA calculation was not needed.

METHOD

Independent Component Analysis and Extraction of CJD-Related Components

Independent component analysis is a statistical method that has been developed to extract independent signals from a linear mixture of sources. Let $\mathbf{X}$ denote the measured data with m and n being the number of channels and the number of data samples, respectively. In the context of ICA, $\mathbf{X}$ is assumed to be linear

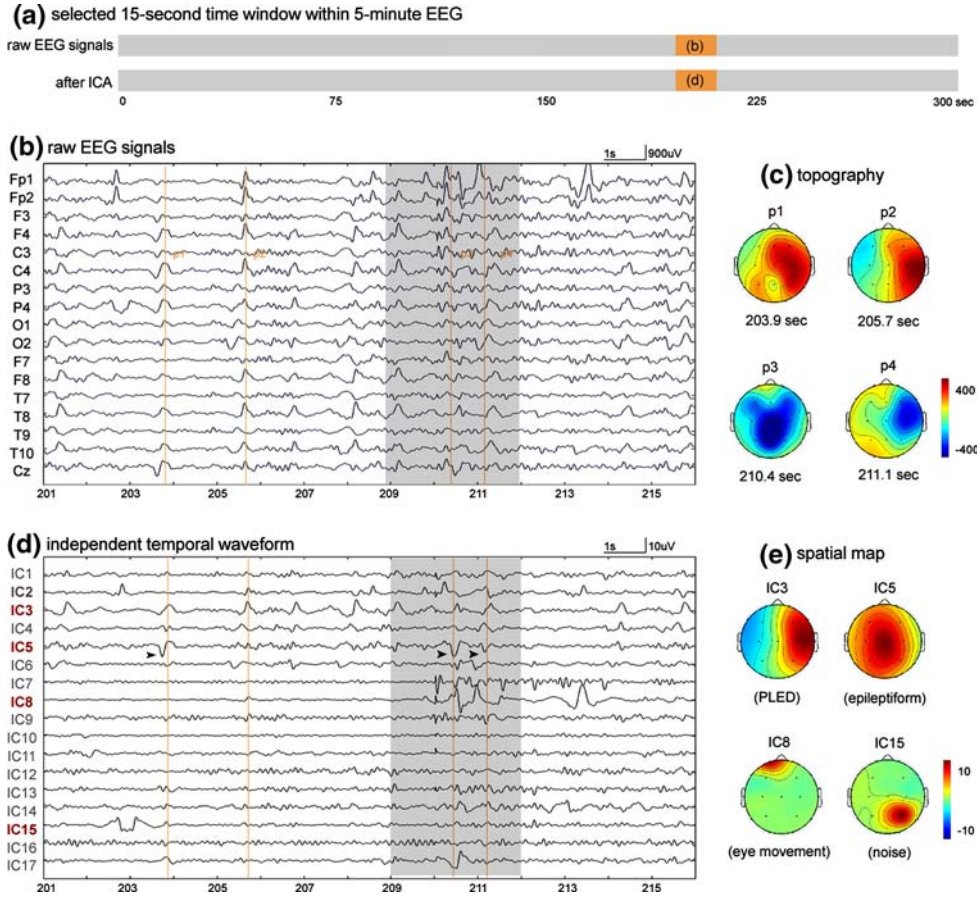

FIGURE 4. The third selected EEG segment and ICA results from patient 1. (a) The 15-second time window (201–216 s) used to display results in (b) and (d). (b) The illustration of a 15-s segment where signals in the shaded areas were severely contaminated by large eye movements and environmental noises. (c) The topographical maps generated at four peak time points p1, p2, p3 and p4 (vertical lines in b) of four waves in IC3 at 203.9, 205.7, 210.4, and 211.1 s. (d) The 17 decomposed ICs show that diseased-related patterns were PLEDs (IC3) and epileptiforms (IC5) and the artifacts were eye movements (IC8) and noise (IC15). (e) The corresponding spatial maps of IC3, IC5, IC8, and IC15.

TABLE 1. Clinical data of probable CJD patients.

Patient	Gender	Age at onset	Disease onset	Clinical presentation	Original EEG report
1	M	73 y/o	6	Memory impairment	PLED, DBS 7 Hz
2	M	74 y/o	9	Memory impairment	FIRDA, DBS 7–8 Hz
3	M	85 y/o	4	Memory impairment	PLED, DBS 6–7 Hz
4	M	52 y/o	5	Memory impairment	DBS 4–5 Hz
5	M	80 y/o	3	Memory impairment	Periodic epileptiform

Disease onset time: weeks before the first admission. DBS: diffuse background slowing.

combinations of k unknown independent components and can be expressed as

$$\underset{m\times n}{\mathbf{X}} = \underset{m\times k}{\mathbf{A}} \cdot \underset{k\times n}{\mathbf{S}}, \tag{3}$$

where $\mathbf{S}$ contains k independent sources with the same data length as $\mathbf{X}$, and $\mathbf{A}$ is a constant mixing matrix with the kth column representing the spatial weights corresponding to the kth component of $\mathbf{S}$. Given the measurement $\mathbf{X}$, ICA techniques attempt to recover both the mixing matrix $\mathbf{A}$ and the independent sources $\mathbf{S}$. In the present study, all calculations were performed using the FastICA algorithm.[11,23] The FastICA technique first removes means of the row vectors in the $\mathbf{X}$ matrix and then uses a whitening procedure, implemented by Principal Components Analysis,[11] to transform the covariance matrix of the zero-mean data into an identity matrix. In the next step, FastICA

searches for a rotation matrix to further separate the whitened data into a set of components, which are as mutually independent as possible. In combination with previous whitening process, the matrix $\mathbf{X}$ is transformed into a matrix $\mathbf{S}$ via an un-mixing matrix $\mathbf{W}$, i.e.,

$$\underset{k\times n}{\mathbf{S}} = \underset{k\times m}{\mathbf{W}}\,\underset{m\times n}{\mathbf{X}} \tag{4}$$

so that rows of $\mathbf{S}$ are mutually independent. The fixed-point method for solving $\mathbf{W} = (\mathbf{w}_i,...,\mathbf{w}_k)^{\mathrm{T}}$ in the FastICA, where k is the number of independent sources, can be summarized as follows[11]:

For $i = 1{:}\ k$,

1. Randomly choose a weighting vector w_i.
2. Let $w_i^+ = E\{xg(w_i^{\mathrm{T}}x)\} - E\{g'(w_i^{\mathrm{T}}x)\}w_i$, where $g(u) = \tanh(c\cdot u)$, $1 \le c \le 2$
3. Let $w_i = w_i^+/\left\|w_i^+\right\|$
4. Go back to step 2 if not converge.
5. Decorrelation by Gram–Schmidt-like scheme, Let $w_i = w_i - \sum_{j=1}^{i-1} w_i^{\mathrm{T}} w_j w_j$
6. Renormalize $\mathbf{w}_i$, Let $w_i = w_i/\|w_i\|$

end

Since EEG can be considered as a linear combination of electric brain activities,[5] we employed ICA to extract the disease-related components from the EEG of five patients. In this study, each pre-processed epoch was arranged across m channels ($m = 17$) and n sampled points ($n = 250{*}300$) into a $m \times n$ matrix $\mathbf{X}$. The ith row contains the observed signal from the ith EEG channel, and the jth column vector contains the observed samples at the jth time point across all channels. FastICA was applied on each pre-processed epoch to resolve the $\mathbf{W}$ and $\mathbf{S}$. After estimating the un-mixing matrix $\mathbf{W}$, we can recover the temporal waveforms by applying the inverse matrix of $\mathbf{W}$ on both sides of Eq. (4) to yield

$$\underset{m\times n}{\mathbf{X}} = \underset{m\times k}{\mathbf{W}^{-1}} \cdot \underset{k\times n}{\mathbf{S}}, \tag{5}$$

where $\mathbf{W}^{-1}$ is the best estimation of the mixing matrix $\mathbf{A}$ in Eq. 3. In the cocktail-party problem, a popular example of ICA model, the kth row of $\mathbf{S}$ represents the voice from the kth speaker, and the element of mixing matrix $\mathbf{A}$ in the mth column and kth row, i.e., $\mathbf{a}_{\mathrm{mk}}$, represents the weighting of the voice from the kth speaker recorded in the mth microphone. In other words, the kth column of $\mathbf{A}$ represents the weightings of the voice of kth speaker at each microphone. In this study, $\mathbf{S}$ represents the time sequences of activation sources, i.e., temporal waveforms of ICs in Figs. 2–5, and $\mathbf{A}$ stands for the weighting of sources recorded from electrodes. Since $\mathbf{W}$ is the estimated un-mixing matrix, each column in $\mathbf{W}^{-1}$ represents a spatial map describing the weightings of the corresponding temporal component at each EEG channel. These spatial maps will hereinafter be referred to as IC spatial maps. The validation of applying ICA to decompose EEG data has been addressed in the pervious studies.[10,13–18,22,23,26] In this study, we have also varied the data length, namely 1-, 2-, 3-, 4-, and 5-min epoch of data, to evaluate the performance of ICA and applied PCA on the same data sets for comparing their results on the feature extraction.

Bayesian Information Criterion (BIC)

We have adopted the BIC,[2,9,19] which was based on the estimation of posterior probability $P(X|A,k)$ given the number of sources k and the observed data $\mathbf{X}$, to estimate the number of sources. The posterior probability was the function of $\mathbf{A}$ given by

$$P(X|A,k) = \prod_k \frac{1}{\sqrt{|2\pi\Lambda_k|}} \left(\frac{1}{|\mathbf{det}(\mathbf{A})|}\right)^{\mathrm{T}} \cdot \exp\left(-\frac{1}{2}\sum_{t,t'} \hat{S}_{k,t}(\Lambda_k^{-1})_{t,t'}\hat{S}_{k,t'}\right), \tag{6}$$

where the notation $\hat{S}_{k,t}$ was the sources estimated from $\mathbf{A}$ and $\mathbf{X}$, $\hat{S}_{k,t} = \sum_l (A^{-1})_{k,l}X_{l,t}$, Λ_k was the covariance matrix of sources and t was the time point. In theory, the number of sources that produced the maximal posterior probability would be selected since the predicted model was best fit to the observed data.

RESULTS

Determination of the Number of Sources

The numbers of sources ranging from 2 to 17 (the number of channels) were introduced to compute the posterior probabilities and the results in Fig. 6 demonstrated that values of posterior probabilities were comparable when N was between 12 and 17. In fact, the resultant CJD-related components were also comparable when N varied from 12 to 17. Instead of using the BIC for determining the number of sources, we simply used the number of channels as the number of sources, as suggested by the previous studies.[10,14–18,26]

CJD-Related Feature Extraction

We have observed that the distinct disease-related patterns were likely to occur in different time windows. Three 15-s windows (Figs. 2a, 3a, and 4a) were selected to illustrate the ICA results obtained from a 5-min EEG

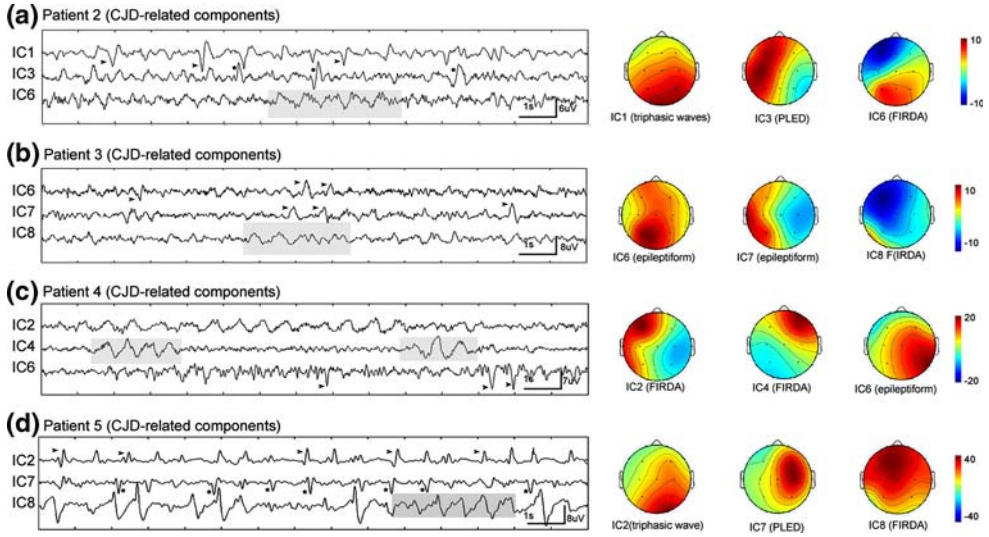

FIGURE 5. Summarized ICA results from patient 2 to patient 5. Each panel shows the selected ICs and corresponding spatial maps for one patient. (a) The ICA results display generalized triphasic waves (IC1), PLEDs lateralized to the left hemisphere (IC3), and slow waves at delta frequency (shaded area of IC6). (b) The ICA results show epileptiforms (IC6, IC7) and FIRDA (shaded area of IC8). (c) The ICA results show the prominent FIRDA over left frontal-temporal area (IC2) and right frontal region (shaded area of IC4), and epileptiforms on the right temporal-occipital lobe (IC6). (d) The ICA results show periodic triphasic waves on the right occipital lobe (IC2), the PLEDs on the right frontal-central area (IC7), and the diffused delta waves (IC8).

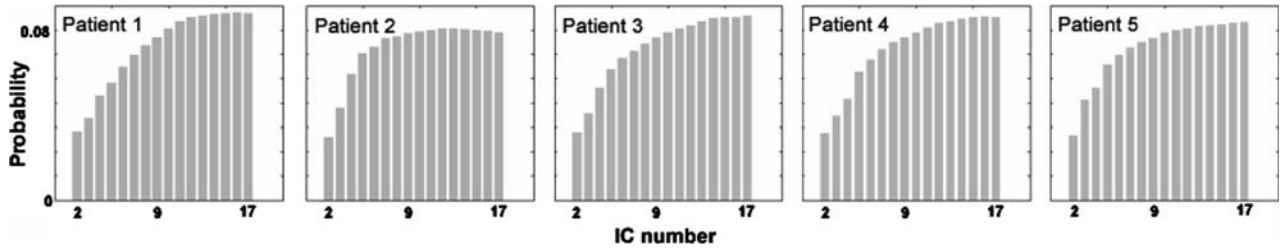

FIGURE 6. The numbers of sources estimated by using the Bayesian information criterion (BIC) from patient 1 to patient 5. Each panel shows the estimated posterior probabilities (histograms) of a patient. The numbers of sources range from 2 to 17 (the number of channels) were given for computing the posterior probabilities (Eq. 6). It is evident that all the estimated posterior probabilities are comparable in each plot when the source numbers are between 12 and 17.

data. The resultant independent temporal waveforms (patient 1, 73 y/o) were presented in Figs. 2d, 3d, and 4d, respectively, and the corresponding spatial maps elucidating CJD-related characteristics or artifacts were depicted in Figs. 2e, 3e, and 4e, respectively. The CJD-related components shown in Figs. 2d, e, 3d, e, and 4d, e are the PLEDs lateralized to the right hemisphere (IC3), triphasic waves on the occipital lobe (IC4), and the PLEDs (IC3) as well as the epileptiforms covering the whole brain (IC5), respectively. The component IC2 was the artifact caused by eye blinks since the spikes occurred intermittently with irregular shapes and large weights exhibited in the prefrontal area of the corresponding spatial map. Similarly, IC8 was identified as an artifact due to left eye movements. The remaining ICs may correspond to spontaneous brain activities irrelevant to CJD or artifacts and were not taken into account in the analysis.

Figure 5 summarizes the individual CJD-related components from the other patients. Each panel shows the selected temporal independent components and the corresponding spatial maps for one patient. The ICA results from patient 2 (74 y/o), display generalized triphasic waves (IC1), PLEDs lateralized to the left hemisphere (IC3), and slow waves at delta frequency (shaded area of IC6) (Fig. 5a). In Fig. 5b, epileptiforms (IC6, IC7) and FIRDA (shaded area of IC8) were resolved from patient 3 (85 y/o). Figure 5c shows the prominent FIRDA over the left frontal-temporal area (IC2) and the right frontal region (shaded area of IC4), and epileptiforms on the right temporal-occipital lobe (IC6) from patient 4 (52 y/o). Finally, Fig. 5(d) displays that the positive periodic triphasic waves appear predominantly on the right occipital lobe (IC2), the PLEDs on the right frontal-central area (IC7), and the diffused delta waves (IC8) from patient 5 (80 y/o).

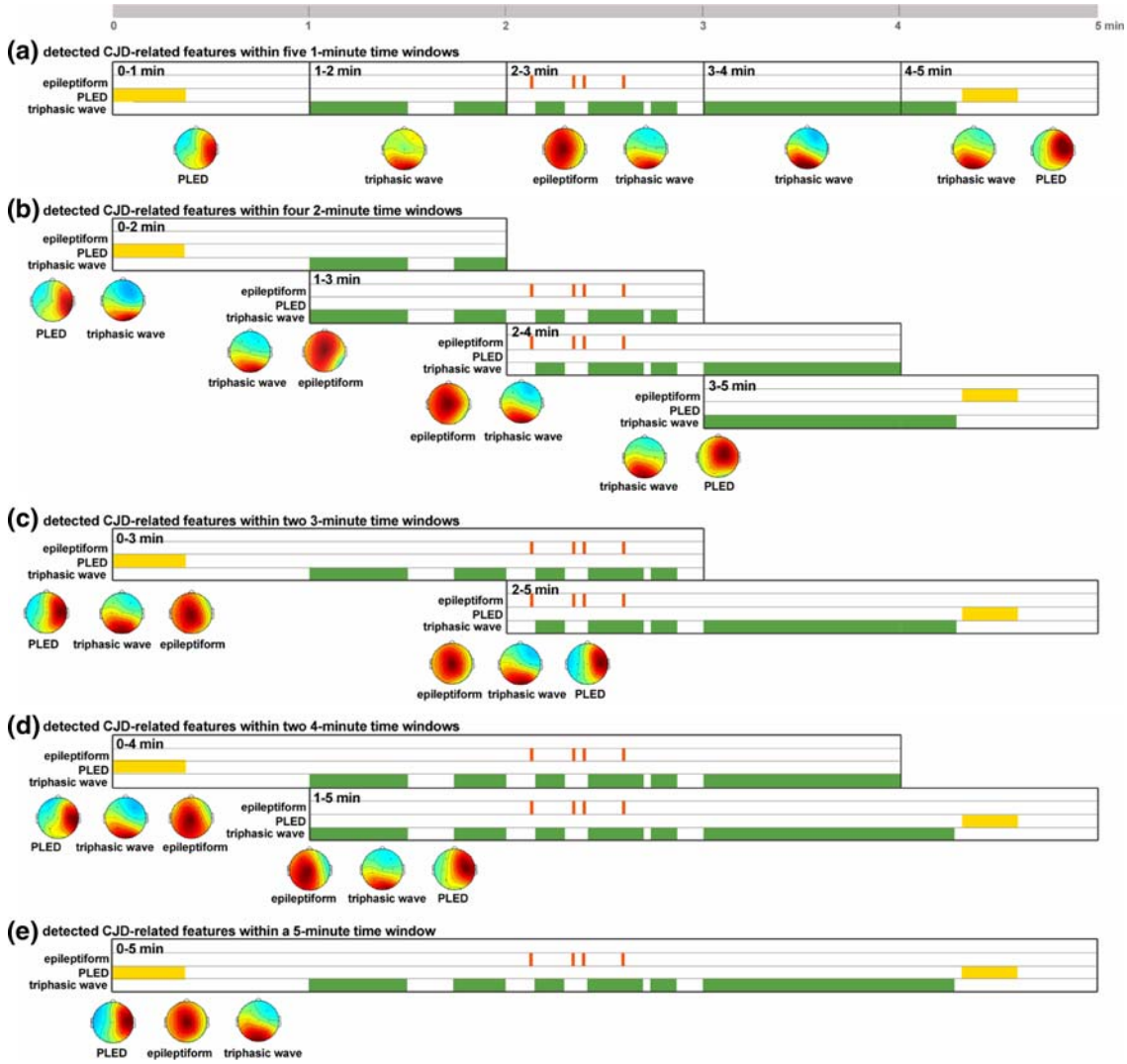

FIGURE 7. Performance of ICA when the 1-, 2-, 3-, 4-, and 5-min epochs of data were analyzed. The bars with different colors in the panels (a) to (e) represent the time periods during which features were resolved, namely, the epileptiform, PLED, and triphasic waves. It can be seen that the ICA results remained unchanged under various data lengths where the same CJD-related patterns repeatedly appeared. Specifically, the PLED presents in the first 20 s within the 1st minute and in the 17th–35th seconds in the 5th minute of the epoch (see the *yellow bars* in the 1st and 5th windows in (a), 1st and 4th windows in (b), 1st and 2nd windows in (c), 1st and 2nd windows in (d), and in (e)). The epileptiform were detected within the 3rd window in (a), 2nd and 3rd windows in (b), 2nd and 3rd windows in (c), 1st and 2nd windows in (d), and in (e) (see *orange bars*). Finally, the triphasic waves can be observed across from the 2nd to the 5th windows in (a), which also appeared in the 1st–4th windows in (b), 1st–2nd windows in (c), 1st–2nd windows in (d), and in (e) (see *green bars*). It should be noted that not only the temporal features preserved the same waveforms and durations, but also the three corresponding spatial maps remained resemble.

Figure 7 shows the results when the 1-, 2-, 3-, 4-, and 5-min epochs of data were analyzed by ICA. The bars with different colors in the Figs. 7a–7e represent the time periods during which features were resolved, namely, the epileptiform, PLED, and triphasic waves. It can be seen that the ICA results remained unchanged under various data lengths where the same CJD-related patterns repeatedly appeared. Specifically, the PLED presents in the first 20 s within the first minute and in the 17th–35th seconds in the 5th minute of the epoch (see the yellow bars in the 1st and 5th windows in (a), 1st and 4th windows in (b), 1st and 2nd windows in (c), 1st and 2nd windows in (d), and in (e)). The epileptiform were detected within the 3rd window in (a), 2nd and 3rd windows in (b), 2nd and 3rd windows in (c), 1st and 2nd windows in (d), and in (e) (see orange bars). Finally, the triphasic waves can be observed across from the 2nd to the 5th windows in (a), which also appeared in the 1st–4th windows in (b), 1st–2nd windows in (c), 1st–2nd windows in (d), and in (e)

(see green bars). It should be noted that not only the temporal features preserved the same waveforms and durations, but also the three corresponding spatial maps remained resemble (see Fig. 7). Similar results have been obtained from other patients (not shown).

Feature Extraction by PCA

It has been reported that the use of ICA under the assumption of source independence can separate more realistically neurophysiologic signals in comparison with the principal component analysis (PCA).[10,12] Since the EEG signals induced by eye blinking or contaminated by electrical noise usually present far larger variances than physiological signals, the covariance-based PCA decomposing procedure is inferior to ICA for resolving meaningful brain activities. As shown in the Fig. 8b where the same time window in Fig. 4a was selected, the temporal waveforms of the first four principal components (eigenvectors corresponding to the first four largest eigenvalues) merely exhibit the preservation of the most power of the original signals. None of them extracted the evident eye-blinking artifacts or CJD-related features from the raw EEG as compared to the ICA results in Fig. 4.

DISCUSSION

This study aims to extract the CJD-related waveforms in conjunction with the spatial dominances from the EEG recordings for the early diagnosis of CJD. Our results demonstrate that ICA is an effective tool for distinguishing FIRDA, PLEDs and PSWCs from EEG recordings in the early stage of CJD (Figs. 2d, e–4d, e, and 5) with dominance in each corresponding spatial map being revealed. In comparison with the raw EEG data in the shaded areas in Figs. 2b–4b, where the CJD-related waveforms were severely smeared by the large potentials of eye movements, three PLEDs, four triphasic waves, and two epileptiforms can be evidently recovered in the shaded areas of IC3 in Fig. 2d, IC4 in Fig. 3d and IC5 in Fig. 4d, respectively. In addition, it should be noted that any 5-min IC waveform only corresponds to a single spatial map and the predominant region for IC3, IC4, and IC5 are manifested in Figs. 2e, 3e, and 4e, respectively. On the contrary, the topographical maps produced from the peak times of the similar waveforms in the raw data varied from one to another. To illustrate this, we particularly chosen four peak times of the disease-related IC waveforms and displayed the topographical maps based on the raw EEG at these peak times. As shown in the vertical lines in Figs. 2b or 2d, four peak time points p1, p2, p3 and p4 of four waves in IC3 at 3.3, 5.1, 9.6 and 10.9 s were selected and the corresponding topographical maps produced from the raw data presented distinct patterns (Fig. 2c), which were difficult to interpret for further analysis. Similar phenomenon and difficulty can be seen in Figs. 3c and 4c.

Another salient feature of ICA is that, even a CJD-related wave hid at different time windows and obscured across multiple channels, ICA is effective to extract such waveforms from different channels into a single independent component, as illustrated by IC3 in Figs. 2d, e and Figs. 4d, e where repeated waves of PLEDs were identified in IC3 which occurred during 2–17 and 201–216 s. Besides, muscular artifacts and

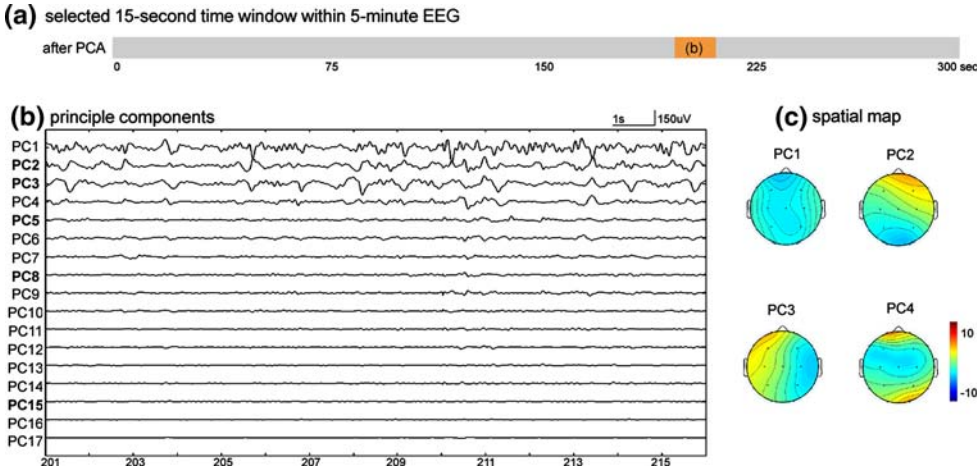

FIGURE 8. The selected EEG segment and PCA results within the same time window as in Fig. 4 from patient 1. (a) The 15-s time window (201–216 s) is used to display results in (b). (b) The 17 decomposed PCs show that the temporal waveforms of the first four principal components (eigenvectors corresponding to the first four largest eigenvalues) merely exhibit the preservation of the most power of the original signals. (c) The corresponding spatial maps of PC1 to PC4. None of them extracted the evident eye-blinking artifacts or CJD-related features from raw EEG as compared to the ICA results in Fig. 4.

environmental noise have been isolated by ICA which were in congruent with previous studies.[14,15,23] The intermittent high amplitude waves induced by eye blinks with maximum over the prefrontal area were presented within IC2 in Figs. 2d, e and 3d, e, large irregular waves caused by eye movements on the left frontal region were within IC8 in Figs. 2 and 3d, e, and environmental noises exhibiting irregularly transient waveforms in a single channel were within IC11 in Fig. 2d, e, IC15 in Figs. 3 and 4d, e.

Most of the previous studies have reported that only one CJD pattern appeared in each stage. The co-occurrence of FIRDA and PLEDs or triphasic waves from the same EEG data has not been explored. For examples, either the FIRDA or FIRDA-like waveforms could be found in the early stage of CJD in most case,[8,25] or the PLEDs appeared initially and were replaced by PSWCs progressively in the middle or late stage.[1,6] The ICA results, nevertheless, illustrated that the FIRDA and PLEDs, or FIRDA and epileptiforms, or FIRDA and triphasic waves concurrently appeared in the same EEG data for each patient. As shown in Table 2, the PLEDs, epileptiforms, and triphasic waves from the 5-min EEG signals of patient 1 can be respectively recovered in IC3, IC5 and IC4, the FIRDA, PLEDs, and triphasic waves in IC6 (shaded area in Fig. 5a), IC3 (stars in Fig. 5a) and IC1 (arrows in Fig. 5a) from patient 2, and in IC8 (shaded area in Fig. 5d), IC7 (stars in Fig. 5d) and IC2 (arrows in Fig. 5d) from patient 5. In addition, FIRDA can be seen in IC8 (shaded area in Fig. 5b) and epileptiforms in IC6 and IC7 (arrows in Fig. 5b) from patient 3, and FIRDA in IC2 and IC4 (shaded area in Fig. 5c) and epileptiforms (arrows in Fig. 5c) in IC6 from patient 4. These findings suggest that the EEG in the early stage of CJD is heterogeneous and concurrent appearance of different CJD patterns should be taken into account in the diagnosis.

It should be noted that only the PSWC had been reported with a 85% specific to the late CJD, the unaccompanied occurrence of each pattern, such as FRIDA, epileptiform, PLED, and triphasic waves, might been seen in other neurological disorders. Therefore, the hypothesis that EEGs of the CJD manifested the co-occurrence of multiple disease-related features was further tested against the Alzheimer's disease (AD) group with five patients who were all male and aged 85, 73, 45, 72, and 79 years old, i.e., age and gender matched with the CJD group. After applying ICA on the AD group, we examined the independent components to detect the disease-related features. No co-occurrence of multiple disease-related features were found in the AD group, except that two ICs were detected to consist of FIRDA in patient 1 and one IC consisted of the epileptiform in patient 4. Based on the co-occurrence of multiple disease-related features exhibited in both groups, the difference between AD and CJD groups was statistically significant (Two-sample Wilcoxon test, $p < 0.05$). Accordingly, the concurrent existence of multiple features presented in the early EEG of CJD patients can be used as an assistive tool for the early diagnosis of CJD.

TABLE 2. The concurrent appearance of different CJD waveforms in the same EEG data from each patient.

Patient	FIRDA	PLEDs	Epileptiform	Triphasic wave
1 (Figs. 2–4)		IC3	IC5	IC4
2 (Fig. 5)	IC6	IC3		IC1
3 (Fig. 5)	IC8		IC6, IC7	
4 (Fig. 5)	IC2, IC4		IC6	
5 (Fig. 5)	IC8	IC7		IC2

The order of same CJD-related components may vary from patient to patient since both the mixing matrix **A** and source matrix **S** are unknown, which allows the change of the order of rows in **S**. To see this, we can substitute a permutation matrix **P** and its inverse into the model, $\mathbf{X} = \mathbf{AS}$, to give $\mathbf{X} = (\mathbf{AP^{-1}})(\mathbf{PS})$. The matrix $\mathbf{AP^{-1}}$ is a new unknown mixing matrix to be solved by the FastICA algorithm[11] and the rows of **PS** are original sources but in different order because each row or column in **P** consists of only one nonzero element with value 1. It is much easier to detect the CJD-related patterns from the unmixed signals rather than from the obscured mixing signals as illustrated in Figs. 2–4, although the same CJD-related sources would occur at different channels among patients. In addition, we found that the ICs consisting of larger spikes, such as irregular waveforms and bursts, tended to be decomposed earlier from the mixing signals in the calculation of FastICA. All the CJD-related features, i.e., sharp waves or epileptiform, have been recognized from ICs lower than IC8.

It is noted that the matrix **S** has lower amplitude in comparison with the matrix **X**. Such an amplitude difference comes from the nature of the linear mixing model and the algorithm of FastICA. Based on the vector form of the model $x_j = a_{j1}s_1 + \cdots + a_{ji}s_i + \cdots$, it can be rewritten into the form $x_j = a_{j1}s_1 + \cdots + (a_{ji}\alpha^{-1})(\alpha s_i) + \cdots$, where α is any arbitrarily nonzero scalar. In other words, the solutions of mixing **A** and source matrix **S** are not unique since any source s_i can be multiplied by a nonzero scalar which can always be cancelled by dividing the corresponding column of **A** by the same scalar. In order to fix the magnitude of the independent components, each source is restricted to have unit variance in the FastICA calculation.[11] As a result, the resolved matrix **S** has lower amplitude than the matrix **X**.

CONCLUSIONS

We have employed ICA to detect the co-occurrence of multiple CJD-related patterns from the EEG recording for aiding to the early diagnosis. Results demonstrate that ICA is an effective tool for simultaneously recovering the FIRDA, PLEDs, and triphasic waves (early PSWCs) that can be hardly discerned by visual inspection from the contaminated EEG recordings. The concurrent appearance of FIRDA and PLEDs or triphasic waves from the same EEG data suggests that the heterogeneity of EEG in the early diagnosis of CJD should be taken into account.

ACKNOWLEDGMENTS

The study was funded by the Taipei Veterans General Hospital (V96 ER1-005) and National Science Council (NSC 95-2218-E-010-001, NSC 95-2752-B-075-001-PAE, NSC 96-2752-B-010-006-PAE, and NSC 96-2752-B-010-007-PAE).

REFERENCES

[1]Au, W. J., A. J. Gabor, N. Vijayan, and O. N. Markand. Periodic lateralized epileptiform complexes (PLEDs) in Creutzfeldt–Jakob disease. *Neurology* 30:611–617, 1980.

[2]Calamante, F., M. Mørup, and L. K. Hansen. Defining a local arterial input function for perfusion MRI using independent component analysis. *Magn. Reson. Med.* 52:789–797, 2004.

[3]Cambier, D. M., K. Kantarci, G. A. Worrell, B. F. Westmoreland, and A. J. Aksamit. Lateralized and focal clinical, EEG, and FLAIR MRI abnormalities in Creutzfeldt–Jakob disease. *Clin. Neurophysiol.* 114(9):1724–1728, 2003.

[4]Collins, S. J., P. Sanchez-Juan, C. L. Masters, G. M. Klug, C. van Duijn, A. Poleggi, M. Pocchiari, S. Almonti, N. Cuadrado-Corrales, J. de Pedro-Cuesta, H. Budka, E. Gelpi, M. Glatzel, M. Tolnay, E. Hewer, I. Zerr, U. Heinemann, H. A. Kretszchmar, G. H. Jansen, E. Olsen, E. Mitrova, A. Alperovitch, J. P. Brandel, J. Mackenzie, K. Murray, and R. G. Will. Determinants of diagnostic investigation sensitivities across the clinical spectrum of sporadic Creutzfeldt–Jakob disease. *Brain* 129:2238–2240, 2006.

[5]Fisch, B. J. Fisch and Spehlmann's EEG Primer. Amsterdam: Elsevier Science B.V, 1999.

[6]Fushimi, M., K. Sato, T. Shimizu, and H. Hadeishi. PLEDs in Creutzfeldt–Jakob disease following a cadaveric dural graft. *Clin. Neurophysiol.* 113:1030–1035, 2002.

[7]Geschwind, M. D., J. Martindale, D. Miller, S. J. DeArmond, J. Uyehara-Lock, D. Gaskin, J. H. Kramer, N. M. Barbaro, and B. L. Miller. Challenging the clinical utility of the 14-3-3 protein for the diagnosis of sporadic Creutzfeldt–Jakob disease. *Arch. Neurol.* 60:813–816, 2003.

[8]Hansen, H. C., S. Zschocke, H. J. Stürenburg, and K. Kunze. Clinical changes and EEG patterns preceding the onset of periodic sharp wave complexes in Creutzfeldt–Jakob disease. *Acta. Neurol. Scand.* 97:99–106, 1998.

[9]Hansen, L. K., J. Larsen, and T. Kolenda. Blind detection of independent dynamic components. *IEEE Int. Conf. Acoust. Speech Signal Process.* 5:3197–3200, 2001.

[10]Hung, C. I., P. L. Lee, Y. T. Wu, L. F. Chen, T. C. Yeh, and J. C. Hsieh. Recognition of motor imagery electroencephalography using independent component analysis and machine classifiers. *Ann. Biomed. Eng.* 33(8):1053–1070, 2005.

[11]Hyvärinen, A., J. Karhunen, and E. Oja. Independent Component Analysis. New York: John Wieley & Sons, Inc, 2001.

[12]Joyce, C. A., I. F. Gorodnitsky, and M. Kutas. Automatic removal of eye movement and blink artifacts from EEG data using blind component separation. *Psychophysiology* 41:313–325, 2004.

[13]Jung, K. Y., J. M. Kimb, D. W. Kimc, and C. S. Chunga. Independent component analysis of generalized spike-and-wave discharges: primary versus secondary bilateral synchrony. *Clin. Neurohysiol.* 116(4):913–919, 2005.

[14]Jung, T. P., S. Makeig, C. Humphries, T. W. Lee, M. J. Mckeown, V. Iragui, and T. J. Sejnowski. Removing electroencephalographic artifacts by blind source separation. *Psychophysiology* 37:163–178, 2000.

[15]Jung, T. P., S. Makeig, M. Westerfield, J. Townsend, E. Courchesne, and T. J. Sejnowski. Removal of eye activity artifacts from visual event-related potentials in normal and clinical subjects. *Clin. Neurohysiol.* 111:1745–1758, 2000.

[16]Kao, Y. H., W. Y. Guo, Y. T. Wu, K. C. Liu, W. Y. Chai, C. Y. Lin, Y. S. Hwang, A. J. K. Liou, H. C. Cheng, T. C. Yeh, J. C. Hsieh, and M. M. H. Teng. Hemodynamic segmentation of MR brain perfusion images using independent component, Bayesian estimation and thresholding. *Magn. Reson. Med.* 49:885–894, 2003.

[17]Lee, P. L., Y. T. Wu, L. F. Chen, Y. S. Chen, C. M. Cheng, T. C. Yeh, L. T. Ho, M. S. Cheng, and J. C. Hsieh. ICA-based spatiotemporal approach for single-trial analysis of postmovement MEG beta synchronization. *NeuroImage* 20:2010–2030, 2003.

[18]Lee, P. L., J. C. Hsieh, C. H. Wu, T. C. Yeh, S. S. Chen, and Y. T. Wu. The brain computer interface using flash visual evoked potential and independent component analysis. *Ann. Biomed. Eng.* 34(10):1641–1654, 2006.

[19]MacKay, D. J. C. Bayesian model comparison and backprop nets. *Adv. Neural Inform. Process. Syst.* 4:839–846, 1992.

[20]Schröter, A., I. Zerr, K. Henkel, H. J. Tschampa, M. Finkenstaedt, and S. Poser. Magnetic resonance imaging in the clinical diagnosis of Creutzfeldt–Jakob disease. *Arch. Neurol.* 57:1751–1757, 2000.

[21]Stearns, S. D., and R. A. David. Signal Processing Algorithms in Matlab. New Jersey: Prentice Hall P T R, 1996.

[22]Urrestarazu, E., P. LeVan, and J. Gotman. Independent component analysis identifies ictal bitemporal activity in intracranial recordings at the time of unilateral discharges. *Clin. Neurohysiol.* 117(3):549–561, 2006.

[23]Vigário, R., J. Särelä, V. Jousmäki, M. Hämäläinen, and E. Oja. Independent component approach to the analysis of EEG and MEG recordings. *IEEE Trans. Biomed. Eng.* 47(5):589–593, 2000.

[24]Wieser, H. G., K. Schindler, and D. Zumsteg. EEG in Creutzfeldt–Jakob disease. *Clin. Neurophysiol.* 117(5):935–951, 2006.

[25]Wieser, H. G., U. Schwarz, T. Blättler, C. Bernoulli, M. Sitlzler, K. Stoeck, and M. Glatzel. Serial EEG findings in sporadic and iatrogenic Creutzfeldt–Jakob disease. *Clin. Neurophysiol*. 115(11):2467–2478, 2004.

[26]Wübbeler, G., A. Ziehe, B. M. Mackert, K. R. Müller, L. Trahms, and G. Curio. Independent component analysis of noninvasively recorded cortical magnetic DC-fields in humans. *IEEE Trans. Biomed. Eng*. 47(5):594–599, 2000.